

DOI: 10.1002/ ((please add manuscript number))

Article type: Full Paper

Non-conjugated flexible linkers in semiconducting polymers – a pathway to improved processability without compromising device performance

*Bob C. Schroeder, Yu-Cheng Chiu, Xiaodan Gu, Yan Zhou, Jie Xu, Jeffrey Lopez, Chien Lu, Michael F. Toney and Zhenan Bao**

Dr. B. C. Schroeder, Dr. Y.-C. Chiu, Dr. X. Gu, Dr. Y. Zhou, Dr. J. Xu, J. Lopez, C. Lu, Prof. Z. Bao

Department of Chemical Engineering, Stanford University, 443 Via Ortega, Stanford, California 94305, United States

E-mail: zbao@stanford.edu

Dr. X. Gu, Dr. M. F. Toney

Stanford Synchrotron Radiation Lightsource, SLAC National Accelerator Laboratory, Menlo Park, California 94025, United States

Keywords: semiconducting polymer, glass transition temperature, all-polymer solar cell, organic field effect transistor, isoindigo

Semiconducting polymers, in contrast to inorganic silicon, are solution processable and can potentially be printed cost efficiently on flexible large-area substrates. However to do so it is of paramount importance to formulate the polymeric semiconductors into inks with specific viscosities. Herein we present the synthesis of a new highly soluble isoindigo monomer and its incorporation into low bandgap semiconducting polymers. Non-conjugated flexible linkers are introduced into the conjugated backbone in order to modulate the materials processability. The viscoelastic properties of the new polymers are studied in detail by means of rheometry and dynamical mechanical analysis (DMA). The solution viscosity is directly proportional to the content of non-conjugated linkers in the polymer backbone. In organic field-effect transistors (OFETs) maximum hole mobilities of $1.7 \text{ cm}^2 \cdot \text{V}^{-1} \cdot \text{s}^{-1}$ are achieved with the new polymers. Due to the enhanced solubility all-polymer solar cells are fabricated by solution shearing, reaching PCE values of 3.7%.

Introduction

With semiconducting polymers currently achieving charge carrier mobilities exceeding those of amorphous silicon ($\sim 1 \text{ cm}^2 \cdot \text{V}^{-1} \cdot \text{s}^{-1}$), they have the potential to lead the development of future application like flexible displays, stretchable sensors or large area ($> 1 \text{ m}^2$), flexible organic photovoltaics. Besides comparable charge carrier mobilities, the superior mechanical properties and the possibility of solution based deposition makes conjugated polymers superior candidates for large-area applications on flexible substrates. Most high-performing semiconducting polymers have a very strong tendency to aggregate in solution, making it necessary to deposit the materials either from dilute solutions or at elevated temperatures. The most common approach to increase the polymers processability is to decorate the conjugated backbone with solubilising alkyl side chains. Recently, we reported the use of low molecular weight oligomer side chains to enhance the solubility.^[1, 2] Even though these approaches have proven to be extremely successful, the introduction of a large number of long electrically insulating side chains may reduce the inter-chain charge transport as well as hinder the charge transfer from donor to acceptor in organic photovoltaic devices.^[3] Choosing the right combination between side chain structure, length and density along the conjugated backbone is non-trivial and can quickly lead to adverse effects, making the screening process very time consuming.

An alternative approach to solubilising side chains is to increase the disorder along the conjugated backbone and to disturb the molecular aggregation, thus facilitating the solution processability. Increasing the energetic disorder within a conjugated polymer chain can be achieved by introducing large rotational angles along the backbone by homo-coupling six-membered aromatic rings (*i.e.* biphenyl, bipyridine, etc.). Or alternatively by introducing sterically hindered head-to-head couplings into the backbone. In both cases the steric hindrance will lead to an increase in rotational

disorder along the polymer chain and reduced molecular aggregation in solution.^[4] Unfortunately, the increase in rotational disorder with these approaches is not limited to the solution phase, but also translates into the solid state. Because the steric hindrance is ‘locked’ into the molecular structure of the polymer backbone, it is irreversible and leads to poor solid state order and inferior electronic properties. A less explored approach to increase energetic disorder along the polymer chain is to introduce non-conjugated, more flexible segments into the backbone. Introducing flexible linkers increases the polymer’s solubility, but crucially should also allow the polymer chain to pack densely in solid state because the backbone rigidity is not perturbed by sterically induced disorder.

In this paper we investigate how the introduction of flexible linkers into the conjugated backbone influences the opto-electronic properties of the semiconducting polymer and how these changes affect the performance of organic field effect transistors (OFET) and all-polymer solar cells. Keeping in mind that the main advantage of semiconducting polymers over amorphous silicon is their solution processability and their potential for applications on flexible substrates, we will put special emphasis on the characterisation of the polymers’ fluid and viscoelastic properties. Both aspects have been barely studied for semiconducting polymers, but are key parameters to understand in order to achieve high performing printed electronic devices on flexible substrates in the future.^[5]

Results and discussion

Amongst the myriad of available building blocks for low bandgap semiconducting polymers, the isoindigo (**iI**) moiety stands out.^[6] Not only can the **iI** core be synthesized with relative ease via aldol condensation of isatin and oxindole, but the **iI** also shows an outstanding photostability under ambient conditions, a key requirement

for stable organic electronic devices. The small torsional angle between the two oxindole subunits ensures good orbital overlap and leads to strong intermolecular π - π interactions between **II** containing polymer chains.^[7] Even though strong intermolecular interactions are beneficial for charge transport because they help to diminish the energetic disorder along the conjugated backbone, they also tend to reduce the polymer's solubility thus making solution processing more challenging. Two approaches that have been particularly successful in enhancing the solution processability without deterring the charge carrier mobilities have been the introduction of a small mol% of polymeric side chains like polystyrene onto the polymer backbone.^[1] Or alternatively the lengthening of the alkyl side chains by introducing alkyl spacers between the conjugated backbone and the branching point of the solubilising side chain.^[8] Rendering the rigid π -conjugated backbone more flexible and thus more soluble by introducing non-conjugated monomers has been a less explored approach and only a couple of reports can be found in literature.^[9] On the one hand this approach could potentially alter the frontier energy levels of the conjugated polymer. A high mol% of non-conjugated monomer in the polymer backbone would prevent the conjugated segments from attaining their effective conjugation length, thus shifting the ionisation potential (IP), respectively the electron affinity (EA). On the other hand the flexible non-conjugated monomers also provide additional disorder to the otherwise rigid and aggregating polymer chains in solution, thus facilitating the solvation. It is important to stress the difference between the solvated state and the solid state. Even though the polymers with flexible linkers form more stable solutions due to their superior solubility, this does not necessarily imply that the solid state packing will be negatively impacted as well. The thin film formation deposition from polymer solution is a rather complex process governed by many variables. However in a simplified picture, one can assume that during the drying process the polymer

solution will concentrate and from a certain critical concentration threshold onwards, the polymer chain aggregation will be the dominating driving force for the film formation thus resulting again in a more ordered solid state packing motif.

Before investigating the effect of non-conjugated monomers in the polymer backbone on processability and performance, a new highly soluble **ii** monomer was synthesised and incorporated into the fully conjugated polymer (**Pii2T**). In order to maximize the final polymer's processability, we decided to decorate the **ii** core with a non-symmetric side chain, 4-octylhexadecyl. The synthesis of the novel 4-octylhexadecyl side chain and the highly soluble (*E*)-6,6'-dibromo-1,1'-bis(4-octylhexadecyl)-[3,3'-biindolinylidene]-2,2'-dione monomer (**11**) are depicted in **Scheme 1**.

Allyltrimethylsilane (**1**) was acylated with nonanoyl chloride catalysed by bismuth (III) chloride and sodium iodide to yield the corresponding dodec-1-en-4-one (**2**).^[10] After hydroboration of the terminal alkene, the resulting primary alcohol was protected via formation of a *tert*-butyldimethylsilyl ether (**4**). The second alkyl chain branch was introduced via Grignard reaction between dodecylmagnesium bromide and the 1-((*tert*-butyldimethylsilyl)oxy)dodecan-4-one (**4**). In a next step the tertiary alcohol was reduced with chlorodiphenylsilane in the presence of indium trichloride and the silyl ether cleaved by addition of tetra-*n*-butylammonium fluoride.^[11] The isolated 4-octylhexadecan-1-ol (**6**) was converted into the corresponding alkyl iodide (**7**) via Appel reaction and used in the subsequent *N*-alkylation of (*E*)-6,6'-dibromo-[3,3'-biindolinylidene]-2,2'-dione (**10**) to yield the highly soluble isoindigo monomer **11**. Having two non-symmetric alkyl chain branches on the side chain should prevent the side chains from crystallising and by moving the branching point away from the conjugated backbone will enhance the solubility further whilst amplifying intermolecular π - π interactions.

Even though short σ -covalent bridges between π -conjugated systems do break the conjugation, they do not necessarily break the electronic communication because under certain geometric constraints through-bond coupling could be possible.^[12] Besides avoiding these additional coupling effects, one has to ensure that the flexible linker is long enough to allow polymer chain folding. Previous reports on monodisperse alkyl chains suggested that six to ten methylene groups are sufficient to allow chain folding, which is why a hexyl linker was introduced between two thiophene units.^[13] Thiophene was lithiated with *n*-butyllithium and quenched by the addition of 0.5 eq 1,6-dibromohexane to yield 1,6-di(thiophen-2-yl)hexane. Detailed synthetic procedures are provided in the supporting information. To avoid any discrepancies in reactivity between the fully conjugated donor monomer, 5,5'-bis(trimethylstannyl)-2,2'-bithiophene, and the covalently bridged linker, the free α -positions of 1,6-di(thiophen-2-yl)hexane were stannylated. Direct stannylation using *n*-butyllithium and subsequently trimethyltin chloride resulted in a complex reaction mixture containing multiple stannylated products difficult to isolate. Therefore the 1,6-di(thiophen-2-yl)hexane was first brominated with *N*-bromosuccinimide, followed by lithiation and stannylation. The presence of bromine on the α -positions helped to guide the lithiation and as a result the desired 1,6-bis(5-(trimethylstannyl)thiophen-2-yl)hexane monomer could be isolated in good yield and high purity.

Four polymers with different mol% (0, 5, 10 and 20%) of non-conjugated linker were synthesized via Stille cross-coupling polymerization (**Scheme 1**). All polymers were end-capped with phenyl groups and residual palladium was chelated with (E)-*N,N*-diethyl-2-phenyldiazene-1-carbothioamide, before the polymers were purified by extensive Soxhlet extraction in methanol, acetone and hexane.^[14] The polymers were recovered with chloroform from the Soxhlet thimble and recovered as dark blue

fibrous materials after precipitation into methanol. Detailed synthetic polymerization and purification protocols are provided in the supporting information.

All polymers were obtained with similarly high number average molecular weights (M_n) ranging between 26 to 33 kg.mol⁻¹ and reasonably high (≥ 24) degrees of polymerization (DP_n) for conjugated polymers (**Table 1**). Even though the size-exclusion chromatography (SEC) was performed at 180°C in 1,2,4-trichlorobenzene, the fully conjugated reference polymer **PiI2T** showed a slightly higher weight dispersity (D_w) than the other co-polymers. Because inter-chain aggregation is unlikely at such elevated temperatures, the shoulder observed at higher retention times in the SEC trace of **PiI2T** (traces provided in **Figure S2**) is attributed to low molecular weight impurities that could not be removed during the Soxhlet purification due to the lower solubility of **PiI2T** in non-chlorinated solvents.

With the exception of **PiI2T**, all polymers are statistical copolymers. ¹H-NMR studies were performed on the purified polymers to ensure the proper mol% of monomer was incorporated into the polymer. As evidenced from the NMR spectra (**Figure S1**), the experimental integration between the terminal methyl protons and the α -protons of the covalent linker corroborates well within the theoretical values, thus confirming the chemical composition of the polymer chains and similar reactivities of both stannylated monomers, 5,5'-bis(trimethylstannyl)-2,2'-bithiophene and 1,6-bis(5-(trimethylstannyl)thiophen-2-yl)hexane.

The previously reported isoindigo-bithiophene copolymer with shorter 2-octyldodecyl side chains (**PiI2T-Ref**) is soluble in hot chlorinated solvents, but when cooled to room temperature the solutions quickly gel, making the processability rather tedious.^[15] In contrast the **PiI2T-X** polymers with the longer 4-octylhexadecyl side chain solubilized easily in warm (50°C) chlorinated solvents and formed homogeneous solutions (20

mg.mL⁻¹) at room temperature. Given those tremendous differences between the fluid properties of **PiI2T-Ref** and **PiI2T-X** polymer solutions, the viscous behaviour of the different polymer solutions was evaluated by rotational rheometry to understand how the longer side chains and the non-conjugated linker might affect the rheological properties. The flow curves for all polymer solutions (20 mg.mL⁻¹ in 1,2-dichlorobenzene (*o*-DCB) at room temperature) are shown in **Figure 1**. Due to strong intermolecular π - π interactions the **PiI2T-Ref** polymer is strongly aggregating and gelling in solution. As the shear rate is increased, shear thinning is observed for **PiI2T-Ref** and the viscosity quickly drops by one order of magnitude to around 1 Pa.s at 25 s⁻¹. At this shear rate a change in slope can be observed in **Figure 1a**, which is caused by the physical disintegration of the gelled polymer solution under increasing shear stress. The more soluble **PiI2T-X** polymers on the other hand did not show any shear-thinning behaviour, but behave like Newtonian fluids in the investigated range of shear rates. Furthermore, the viscosity of the polymer solutions decreases by increasing the mol% of non-conjugated monomer in the polymer backbone. Whereas the viscosity of the fully conjugated **PiI2T** polymer was measured to be 6.2×10^{-2} Pa.s, the viscosity decreased by one order of magnitude to 2.4×10^{-3} Pa.s when 20 mol% of covalently linked monomer (**PiI2T-20**) were introduced into the polymer backbone. The rheological measurements conclusively show that the introduction of non-conjugated monomers into the otherwise conjugated polymer backbone are an efficient synthetic approach to not only enhance the polymer solubility, but more importantly to tune the viscosity in order to match the specific requirements of the various printing technologies.

Despite all processability improvements, it is well understood that the introduction of σ -linkages into a π -conjugated system reduces the effective conjugation length, leading

to an increase in bandgap caused by shifting the frontier energy levels. To better understand the implications of the non-conjugated linker on the opto-electronic properties of the **PiI2T-X** polymers, the UV-*vis.* absorption spectra in solutions and thin films on glass substrates were recorded (**Figure 2**). A detailed table summarizing the optical properties is provided in the supporting information (**Table S1**). In both cases, two distinctive absorption bands were observed. A higher energy band (Band II) around 420 nm associated to the π - π^* transitions and a broader lower energy band (Band I) ranging from 550 to 800 nm originating from the internal charge transfer (ICT) between the donor and acceptor moieties of the polymer backbone. Band II presents at least three different vibrational peaks (0-0, 0-1 and 0-2) as previously described for **iI** based polymers.^[16] Interestingly the intensity of the different vibrational peaks differs a lot from polymer to polymer and even more so between the solution and the solid state spectra. The intensity of the vibrational peaks in the solution spectra are proportional to the mol% of non-conjugated linker in the polymer backbone. This is not surprising, given that the aforementioned rheological studies already suggested that an increase in covalently linked non-conjugated monomer leads to weaker interchain interactions and as a result better solvated polymer chains in solutions. A similar trend is observed in the UV-*vis.* spectra of the polymers in thin films. The vibrational features are overall more defined in the solid state spectra than in the solution spectra, implying that the introduction of the flexible non-conjugated linker does not dramatically alter the solid state ordering of the **PiI2T-X** polymers, thus giving rise to similar vibrational features.

The most interesting observation however is the absence of any differences in the optical bandgaps (E_g), independent of the mol% of non-conjugated linker introduced into the polymer chain. In a computational study on **iI** containing polymers, Salvatori

et al. found that the effective conjugation length saturates after as little as five repeating units.^[17] These findings would also explain why no shifts in optical bandgaps were observed for the different **PiI2T-X** polymers because the content of non-conjugated monomer in the backbone never exceeded 20 mol%, thus allowing even the **Pi2T-20** polymer to reach its effective conjugation length. The oxidation potentials of all polymers were measured by differential pulse voltammetry (DPV), as well as by cyclic voltammetry (CV), on polymer thin films deposited ITO coated glass slides. The results are summarized in **Table 2** and the corresponding voltammograms are provided in **Figure S3**.

The ionisation potentials of the **PiI2T-X** polymers were estimated to be around -5.56 eV according to the DPV measurements. The values calculated based on the CV measurements were around 0.1 eV higher and showed slightly larger deviations between the different polymers. Knowing that the onset is often poorly defined in CV compared to DPV measurements, the introduced error is consequently also larger leading to the spread of 0.6 eV for the IP_{CV} values. A similar argument holds true with regard to the lower IP values obtained by DPV, in addition the sensitivity of DPV is higher, which could cause the small shift of ~0.1 eV in ionisation potentials observed for the different techniques.^[18] Regardless of the differences caused by experimental setups, the ionisation potentials of the polymers are not significantly influenced by the presence of non-conjugated monomers in the polymer backbone and neither are the electron affinities, which were estimated to be around -3.9 eV.

Physical characteristics of conjugated polymers, like glass transition temperatures (T_g) or melting temperatures (T_m), are often overlooked during material processing even though these parameters could make the difference between an average device and a record breaking one.^[19] There are multiple examples in literature highlighting the

importance of appropriate annealing temperatures above T_g to allow the polymer chains to adopt an equilibrium conformation post-deposition in order to diminish the energetic disorder within the polymer chains and to improve the charge transport in organic field effect transistors (OFET).^[20] A good understanding of the T_g is equally important for high performing organic photovoltaics, especially when considering that multiple components (donor, acceptor, additives etc.) are involved in the formation of the active layer. In case the operating temperature is significantly higher than the T_g , the corresponding decrease in viscosity leads to accelerated diffusion, causing phase separation or crystallisation in the active layer, thus deterring the long term device stability.^[21] Besides the mentioned performance considerations, the potential use of flexible substrates with organic semiconductors, one of the main advantages over inorganic silicon, would allow the fabrication of truly wearable electronics that remain operational even after physical deformation.^[22] However to ensure the intrinsic flexibility of the semiconducting polymers and to allow the polymer chains to reorganize after being submitted to external mechanical stresses, it is crucial to have a good understanding of the T_g of the polymer in question.

In contrast to the stiff and rigid backbone of the fully conjugated **Pi2T** polymer, the introduction of the malleable σ -linked monomers should alter the physical and mechanical properties of the polymers. All **Pi2T-X** polymers showed exceptional thermal stability ($\geq 350^\circ\text{C}$, data provided in **Figure S4**) during the thermal gravimetric analysis (TGA). The differential scanning calorimetry (DSC) measurements (**Figure 3**) did not show any significant first order transitions in the investigated temperature range (-90 to 300°C). The complete DSC curves of all the polymers are provided in the supporting information (**Figure S5 - S8**). However all samples presented a reproducible second order transition around -40°C depicted in **Figure 3** and with

increasing covalent linker percentage in the polymer backbone the inflection point of this transition shifts from -37°C for **PiI2T** to -45°C for **PiI2T-20**. The glass transition temperature of conjugated polymers varies significantly with the stiffness of the backbone and even though 20 mol% of flexible monomer were introduced into the **PiI2T** polymer backbones, they should still be too rigid to allow glass transition temperatures around -40°C . A more plausible explanation for the observed second order transition at low temperature would be to picture the **PiI2T-X** polymers as “block copolymers” comprised of two different segments, the stiffer conjugated backbone and the highly flexible side chains. With this assumption, the observed second order transitions around -40°C could be related to the alkyl side chains decorating the conjugated backbone, whereas the glass transition associated to the backbone might be too weak to be observed in the DSC experiments due to limited sensitivities.^[23] To verify this hypothesis, the backbone glass transition temperatures were probed by differential alternating current (ac) chip calorimetry, a technique with improved sensitivity ($\text{pJ}\cdot^{\circ}\text{C}^{-1}$).^[24]

The calorimetric ac-chip measurements revealed an additional 2nd order transition at elevated temperatures (50 to 70°C) for the **PiI2T** polymers containing the non-conjugated linker as evidenced from the heating curves depicted in **Figure S9**. In contrast to the aforementioned DSC measurements, no clear trend relating the glass transition temperatures to the mol% of σ -linked monomer in the polymer backbone could be established. Nevertheless, the ac-chip measurements support our hypothesis of two glass transition temperatures within the same conjugated polymer, a more intense beta-transition at sub-zero temperatures (T_{β}) related to the alkyl side chains and a weaker alpha-transition correlated to the conjugated backbone at higher temperatures (T_{α}).

Dynamic mechanical analysis (DMA) was performed on the **PiI2T-X** polymers to confirm the presence of two different glass transition temperatures. The sample preparation of semiconducting polymers for DMA analysis however is not trivial because free-standing conjugated polymer thin films are extremely brittle and difficult to handle. To circumvent this problem, thin films ($\pm 1 \mu\text{m}$) of **PiI2T-X** polymers were drop-casted on supportive polyimide films (600 nm), which allowed us to study the structural reorganization of the conjugated polymers by means of DMA.^[25] The DMA results for **PiI2T** are shown in **Figure 3b** and detailed DMA curves for all other polymers are provided in the supporting information (**Figure S10 - S12**). Similar to the results obtained by ac-chip measurements, all investigated **PiI2T-X** polymers present two maxima in their corresponding $\tan \delta$ curves. One more intense peak at around -30°C originating from the alkyl side-chain relaxation and a significantly weaker peak at more elevated temperatures ($40 - 60^\circ\text{C}$) related to the glass transition of the conjugated polymer backbone. Once again the introduction of the flexible linker does not seem to have a significant effect on the glass transition temperatures.

Even though the mol% of σ -bonded linker in the conjugated backbone is not significantly affecting the mechanical properties of the different polymers, a dramatic impact on the charge transport properties however should be anticipated. To get a better understanding of the impact of the non-conjugated linker on the charge carrier mobilities in the **PiI2T-X** polymers, bottom-gate top-contact organic field effect transistors were fabricated. A typical transfer curve of **PiI2T-5** and the hole mobility evolution as a function of annealing temperature are presented in **Figure 4**. Detailed device characteristics are given in **Table 3** and additional transfer curves are provided in the supporting information (**Figure S13 – S16**). The highest hole mobilities of all **PiI2T** polymers were recorded for the fully conjugated **PiI2T** polymer. Hole mobilities

of $1 \text{ cm}^2 \cdot \text{V}^{-1} \cdot \text{s}^{-1}$ were achieved for as-cast thin films and could be further improved to above $2 \text{ cm}^2 \cdot \text{V}^{-1} \cdot \text{s}^{-1}$ by thermal annealing of the thin films. The nearly featureless DSC curves made the choice of annealing temperatures difficult. The polymer films were annealed at 150°C and 200°C , primarily to drive solvent impurities out of the films and to increase the film crystallinity, given that both annealing temperatures are significantly higher than the identified T_g , but at the same time well below the decomposition temperatures measured by TGA. The measured mobilities are in good agreement with previous reports on charge carrier mobilities in isoindigo containing semiconducting polymers.^[26] Interestingly the introduction of non-conjugated units into the backbone did not affect the hole carrier mobilities as dramatically as one would have expected. Both **PiI2T-5** and **PiI2T-10** showed comparable hole mobilities to the fully conjugated **PiI2T** in as-cast devices. The charge carrier mobilities of both polymers could be further increased upon thermal annealing, approaching $1 \text{ cm}^2 \cdot \text{V}^{-1} \cdot \text{s}^{-1}$, and exceeding this in case of **PiI2T-5**. The performance of **PiI2T-20** based transistors however was lower and hole mobilities were stagnating around $0.2 \text{ cm}^2 \cdot \text{V}^{-1} \cdot \text{s}^{-1}$ independent of thermal annealing. Considering the limited conjugation along the polymer backbone in **PiI2T-20**, it is not surprising that the intrachain charge transport in this material is limited and that the charge transport mechanism is strongly dependent on slower interchain hopping, reflected in the overall lower carrier mobilities. Nevertheless, the non-fully conjugated polymers achieved unexpectedly high carrier mobilities.

Grazing incidence x-ray diffraction (GIXD) experiments were performed on all **PiI2T-X** thin films in order to probe the molecular packing, which most likely is one of the reasons for the excellent charge transport in these materials. The GIXD images of the different thin films are shown in **Figure 5** and the key parameters summarized in

Table 4. All films show a strong preference for edge-on orientation as evidenced by the intense out of plane ($h00$) alkyl diffraction. Of all pristine films, **PiI2T** is the most disordered sample with a larger fraction of face-on oriented crystallites, as suggested by the arc shape of the ($h00$) peaks and the appearance of a weak (010) peak along the $q_{x,y}$ axis. Nevertheless, upon thermal treatment the order and crystallinity of all films increase as shown in **Figure S18**, depicting the decrease in full width at half maximum (FWHM) as a function of annealing temperature. Furthermore, the crystallite orientation changes and all samples show a strong preference for edge-on orientation after thermal annealing. Furthermore, we believe that the high negative V_{th} values observed in OFET measurements originate from the edge-on orientation of the various **PiI2T-X** polymers. Due to the lamellar orientation of the polymers, the long alkyl side chains are perpendicular to the hole-injection electrode, thus inducing an injection barrier between the source and channel, leading to more negative V_{th} .

In addition to the orientation, the studied samples show interesting differences in lamellar stacking distances (**Table 4**) and the effect of thermal annealing on this spacing. Firstly, it is noteworthy that the lamellar spacing is inversely proportional to the amount of covalently bridged linker in the conjugated backbone. Whereas the lamellar stacking distance for the pristine **PiI2T** was measured to be 24.36 Å, only 23.67 Å were observed for the pristine **PiI2T-20** film. The exact origin for this decrease is not fully understood, however we speculate it might be related to the film forming dynamics and side chain density along the polymer backbone. As previously discussed, solutions of **PiI2T** are significantly more viscous than solutions of the non-fully conjugated **PiI2T-X** polymers. This increased viscosity is the result of polymer chain aggregation in solution, thus limiting the free movement of the solvated polymer chains. The aggregated polymer chains are “locked” into a conformation that does not

reflect the thermodynamic equilibrium, but rather a pseudo-equilibrium. Upon film deposition, the aggregated polymer chains will not be mobile enough to pack in the energetically most favourable motif, but will be kinetically trapped upon solvent evaporation, leading to a larger and non-ideal lamellar stacking distances. Polymer solutions of the non-fully conjugated polymers on the other hand are less viscous, which facilitates the packing of the polymer chains, thus yielding smaller lamellar stacking distances and smaller FWHM. The assumption that film forming dynamics and solution viscosities largely dictate the different lamellar stacking distances is also reflected in the changes of lamellar spacing distances upon thermal annealing. The decrease in d -spacing distance upon temperature treatment is the most pronounced in **Pi2T**, in which a decrease of nearly 0.2 Å is observed. With increasing flexible linker in the backbone the effects of the thermal annealing on the lamellar spacing decrease and a difference of only ± 0.05 Å is measured between the pristine and annealed (200°C) **Pi2T-20** films. The decreasing dependence of thermal annealing on the d -spacing distances is most likely again related to the hypothesis that pristine **Pi2T** films are partially quenched in a non-ideal packing motif after deposition, hence will relax more upon thermal treatment.

In addition to the discussed film forming dynamics, the side chain density along the polymer backbone has to be taken into account when rationalizing the different lamellar stacking distances. Knowing that all **Pi2T-X** polymers have very similar molecular weights, the side chain density along the polymer backbone decreases with increasing flexible linker content.^[27] This could have a significant influence on the solid state packing of the different polymers and give rise to changes in the d -spacing. In case of **Pi2T**, every repeating unit contains two side chains and there is no “dead volume” along the polymer backbone available to accommodate those side chains in

order to achieve a denser packing motive, thus resulting in larger lamellar stacking distances. With increasing non-conjugated linker in the polymer backbone however, the side chain density along the backbone decreases and the “dead-volume” increases. Therefore, it might be possible to have partial interdigitation of the side chains of adjacent polymer chains, which would lead to a denser packing motif and smaller lamellar stacking distances as observed for **PiI2T-5**, **PiI2T-10**, respectively **PiI2T-20**.

One of the major design aims of the **PiI2T-X** polymers was to enhance the processability of the polymers, whilst maintaining their initial outstanding performance. In order to take full advantage of the enhanced solubility, all polymer solar cells were fabricated via solution shearing, a technology able to coat large area substrates.^[28] For all-polymer solar cells the molecular structure of both donor and acceptor polymers, as well as the solubility and the aggregation in solution of the polymers are of paramount importance in order to achieve high performing photovoltaic devices. A perylene tetracarboxylic diimide based polymer, namely **P(TP)**, was chosen as electron accepting polymer because it was previously used in conjunction with isoindigo based polymers and the corresponding devices showed excellent power conversion efficiencies.^[29] The *J-V* curves and EQE spectra of all **PiI2T-X** based photovoltaic devices are presented in **Figure 6**. All devices were fabricated in an inverted structure ITO/ZnO/PiI2T-X:P(TP)/MoO₃/Ag on a ITO coated glass substrate.

The recorded V_{OC} values of all organic photovoltaic (OPV) devices are similar, which is not unexpected considering that the HOMO energy levels of all **PiI2T-X** polymers are nearly identical. The differences are slightly more significant for the measured J_{SC} values, which range from 7.77 to 8.51 mA.cm⁻² without an identifiable trend. The FF values are nearly identical for all polymers, except **PiI2T-20** for which the FF drops to

0.44. Consequently, the lowest PCE (3.0%) was also obtained for the **PiI2T-20** device. For all other devices the PCEs exceeded 3.0% with the highest value of 3.7% reached for the **PiI2T-5** device. The performance differences observed between the various devices, origin from differences in J_{SC} values, which most likely are caused by morphological differences in the nanoscale phase separation of the BHJ layer. This finding provides strong evidence for the efficacy of the non-conjugated linker approach to not only influence the material processability, but to also be an effective tool to enhance all-polymer solar cell performance.

Conclusion

In summary, we synthesized a new highly soluble isoindigo monomer with a non-symmetric side chain, 4-octylhexadecyl, and incorporated it into a series of conjugated low-bandgap polymers. Furthermore, the insertion of a flexible non-conjugated monomer into the polymer backbone proved to be a highly efficient approach to further enhance the polymers solubility and processability. Rheology measurements revealed that the polymer solution viscosity is directly proportional to the amount of covalent linker in the polymer backbone. Contrary to common belief, outstanding performances in organic field effect transistors with hole mobilities exceeding $1 \text{ cm}^2 \cdot \text{V}^{-1} \cdot \text{s}^{-1}$ were achieved, despite the non-fully conjugated character of the polymers. GIXD studies revealed that the excellent carrier mobilities are most likely the result of the exceptionally high degree of order found for all **PiI2T-X** polymers. The excellent processability of all polymers proved to be a key factor in order to use the new polymers as donor materials in all-polymer solar cells. PCEs of 3% were routinely measured, with the best devices attaining values of 3.7% in case of **PiI2T-5**. The incorporation of covalent linkers into the polymer backbone proved to be an exceptionally versatile tool not only to modulate the fluid and viscoelastic properties,

but also to tweak the device performance; especially in case of all-polymer solar cells, where this new approach could be used to optimize the BHJ morphology.

Supporting Information

Supporting Information is available from the Wiley Online Library and includes Synthetic procedures, polymer NMR spectra, SEC chromatograms, cyclic voltammograms, TGA and additional DSC curves, DMA curves and OFET characteristics.

Acknowledgements

The authors thank Nathan Ging-Ji Wang for performing the high-temperature SEC experiments. BCS acknowledges the National Research Fund of Luxembourg for financial support (Project 6932623). JL acknowledges support by the National Science Foundation Graduate Research Fellowship Program under Grant No. (DGE-114747). XG, MT and ZB thank the National Science Foundation Materials Genome Program (Award No. 1434799). YZ and ZB are grateful to the Office of Navy Research (N00014-14-1-0142). YC and ZB acknowledge support from the National Science Foundation (DMR-1303178). JX and ZB acknowledge support from Samsung Electronics. Use of the Stanford Synchrotron Radiation Lightsource, SLAC National Accelerator Laboratory, is supported by the U.S. Department of Energy, Office of Science, Office of Basic Energy Sciences under Contract No. DE-AC02-76SF00515.

Received: ((will be filled in by the editorial staff))

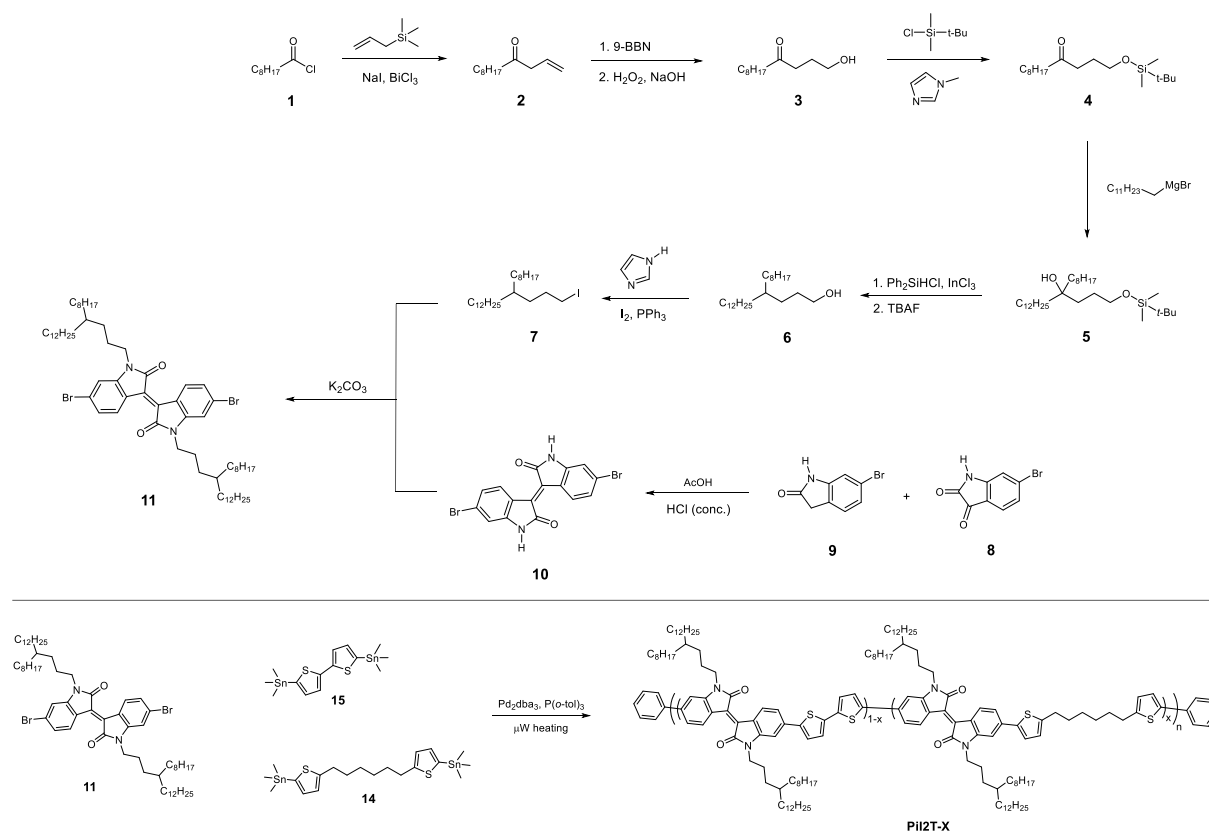
Revised: ((will be filled in by the editorial staff))

Published online: ((will be filled in by the editorial staff))

- [1] L. Fang, Y. Zhou, Y.-X. Yao, Y. Diao, W.-Y. Lee, A. L. Appleton, R. Allen, J. Reinspach, S. C. B. Mannsfeld, Z. Bao, *Chem. Mater.* **2013**, *25*, 4874.
- [2] T. Kurosawa, Y.-C. Chiu, Y. Zhou, X. Gu, W.-C. Chen, Z. Bao, *Adv. Funct. Mater.* **2015**, *n/a*.

- [3] a) T. Lei, J.-Y. Wang, J. Pei, *Chem. Mater.* **2014**, *26*, 594; b) J. Mei, Z. Bao, *Chem. Mater.* **2014**, *26*, 604.
- [4] B. C. Schroeder, S. Rossbauer, R. J. Kline, L. Biniek, S. E. Watkins, T. D. Anthopoulos, I. McCulloch, C. B. Nielsen, *Macromolecules* **2014**, *47*, 2883.
- [5] a) S. R. Forrest, *Nature* **2004**, *428*, 911; b) M. Berggren, D. Nilsson, N. D. Robinson, *Nat. Mater.* **2007**, *6*, 3.
- [6] R. Stalder, J. Mei, K. R. Graham, L. A. Estrada, J. R. Reynolds, *Chem. Mater.* **2014**, *26*, 664.
- [7] L. A. Estrada, R. Stalder, K. A. Abboud, C. Risko, J.-L. Brédas, J. R. Reynolds, *Macromolecules* **2013**, *46*, 8832.
- [8] a) T. Lei, J.-H. Dou, J. Pei, *Adv. Mater.* **2012**, *24*, 6457; b) I. Meager, R. S. Ashraf, S. Mollinger, B. C. Schroeder, H. Bronstein, D. Beatrup, M. S. Vezie, T. Kirchartz, A. Salleo, J. Nelson, I. McCulloch, *J. Am. Chem. Soc.* **2013**, *135*, 11537.
- [9] a) M. Zhao, K. Hashimoto, K. Tajima, *Synthetic Metals* **2013**, *175*, 9; b) A. Gasperini, S. Bivaud, K. Sivula, *Chem. Sci.* **2014**, *5*, 4922; c) Y. Zhao, X. Zhao, Y. Zang, C.-a. Di, Y. Diao, J. Mei, *Macromolecules* **2015**, *48*, 2048.
- [10] a) C. Le Roux, J. Dubac, *Organometallics* **1996**, *15*, 4646; b) B. M. Trost, H. Yang, G. Wuitschik, *Org. Lett.* **2005**, *7*, 4761.
- [11] M. Yasuda, Y. Onishi, M. Ueba, T. Miyai, A. Baba, *J. Org. Chem.* **2001**, *66*, 7741.
- [12] M. Jenart, C. Niebel, J.-Y. Balandier, J. Leroy, A. Mignolet, S. Stas, A. Van Vooren, J. Cornil, Y. H. Geerts, *Tetrahedron* **2012**, *68*, 349.
- [13] G. Grasso, J. J. Titman, *Macromolecules* **2009**, *42*, 4175.
- [14] K. T. Nielsen, K. Bechgaard, F. C. Krebs, *Macromolecules* **2005**, *38*, 658.
- [15] T. Lei, Y. Cao, Y. Fan, C. J. Liu, S. C. Yuan, J. Pei, *J. Am. Chem. Soc.* **2011**, *133*, 6099.
- [16] T. Lei, Y. Cao, X. Zhou, Y. Peng, J. Bian, J. Pei, *Chem. Mater.* **2012**, *24*, 1762.
- [17] P. Salvatori, E. Mosconi, E. Wang, M. Andersson, M. Muccini, F. De Angelis, *J. Phys. Chem. C* **2013**, *117*, 17940.
- [18] A. Bard, L. Faulkner, *Electrochemical Methods: Fundamentals and Applications*, John Wiley & Sons, Inc, **2001**.
- [19] C. Müller, *Chem. Mater.* **2015**, *27*, 2740.
- [20] a) I. McCulloch, M. Heeney, C. Bailey, K. Genevicius, I. MacDonald, M. Shkunov, D. Sparrowe, S. Tierney, R. Wagner, W. Zhang, M. L. Chabinyc, R. J. Kline, M. D. McGehee, M. F. Toney, *Nat. Mater.* **2006**, *5*, 328; b) J. S. Ha, K. H. Kim, D. H. Choi, *J. Am. Chem. Soc.* **2011**, *133*, 10364; c) Z. Chen, M. J. Lee, R. Shahid Ashraf, Y. Gu, S. Albert-Seifried, M. Meedom Nielsen, B. C. Schroeder, T. D. Anthopoulos, M. Heeney, I. McCulloch, H. Sirringhaus, *Adv. Mater.* **2012**, *24*, 647.
- [21] a) S. Bertho, I. Haeldermans, A. Swinnen, W. Moons, T. Martens, L. Lutsen, D. Vanderzande, J. Manca, A. Senes, A. Bonfiglio, *Sol. Energ. Mat. Sol. Cells* **2007**, *91*, 385; b) C. Muller, J. Bergqvist, K. Vandewal, K. Tvingstedt, A. S. Anselmo, R. Magnusson, M. I. Alonso, E. Moons, H. Arwin, M. Campoy-Quiles, O. Inganas, *J. Mat. Chem.* **2011**, *21*, 10676; c) J. Bergqvist, C. Lindqvist, O. Backe, Z. Ma, Z. Tang, W. Tress, S. Gustafsson, E. Wang, E. Olsson, M. R. Andersson, O. Inganas, C. Muller, *J. Mat. Chem. A* **2014**, *2*, 6146.
- [22] a) T. Sekitani, T. Someya, *Adv. Mater.* **2010**, *22*, 2228; b) D. J. Lipomi, *Adv. Mater.* **2015**, *n/a*.
- [23] X. Luo, S. Xie, J. Liu, H. Hu, J. Jiang, W. Huang, H. Gao, D. Zhou, Z. Lu, D. Yan, *Polym. Chem.* **2014**, *5*, 1305.
- [24] H. Huth, A. A. Minakov, C. Schick, *J. Polym. Sci. Part B Polym. Phys.* **2006**, *44*, 2996.
- [25] K.-i. Akabori, K. Tanaka, T. Nagamura, A. Takahara, T. Kajiyama, *Macromolecules* **2005**, *38*, 9735.
- [26] T. Lei, J.-Y. Wang, J. Pei, *Acc. Chem. Res.* **2014**, *47*, 1117.

- [27] X. Zhang, L. J. Richter, D. M. DeLongchamp, R. J. Kline, M. R. Hammond, I. McCulloch, M. Heeney, R. S. Ashraf, J. N. Smith, T. D. Anthopoulos, B. C. Schroeder, Y. H. Geerts, D. A. Fischer, M. F. Toney, *J. Am. Chem. Soc.* **2011**, *133*, 15073.
- [28] Y. Diao, Y. Zhou, T. Kurosawa, L. Shaw, C. Wang, S. Park, Y. Guo, J. A. Reinspach, K. Gu, X. Gu, B. C. K. Tee, C. Pang, H. Yan, D. Zhao, M. F. Toney, S. C. B. Mannsfeld, Z. Bao, *Nat. Commun.* **2015**, *6*.
- [29] Y. Zhou, T. Kurosawa, W. Ma, Y. Guo, L. Fang, K. Vandewal, Y. Diao, C. Wang, Q. Yan, J. Reinspach, J. Mei, A. L. Appleton, G. I. Koleilat, Y. Gao, S. C. B. Mannsfeld, A. Salleo, H. Ade, D. Zhao, Z. Bao, *Adv. Mater.* **2014**, *26*, 3767.



Scheme 1. Synthetic pathway towards the highly soluble **iI** monomer (**11**) and synthesis of **PiI2T-X** polymers via microwave assisted Stille coupling.

Table 1. Chemical composition and molecular weights of the different **PiI2T-X** polymers.

Polymer	x	M_n^a [kg/mol]	M_w^b [kg/mol]	\mathcal{D}_w^c	DP_n^d
PiI2T	0	33	113	3.4	30
PiI2T-5	0.05	33	96	2.9	30
PiI2T-10	0.10	30	81	2.7	27
PiI2T-20	0.20	26	64	2.5	24

^a Number-average molecular weight. ^b Weight-average molecular weight. ^c Weight dispersity defined as M_w/M_n . ^d Degree of polymerization.

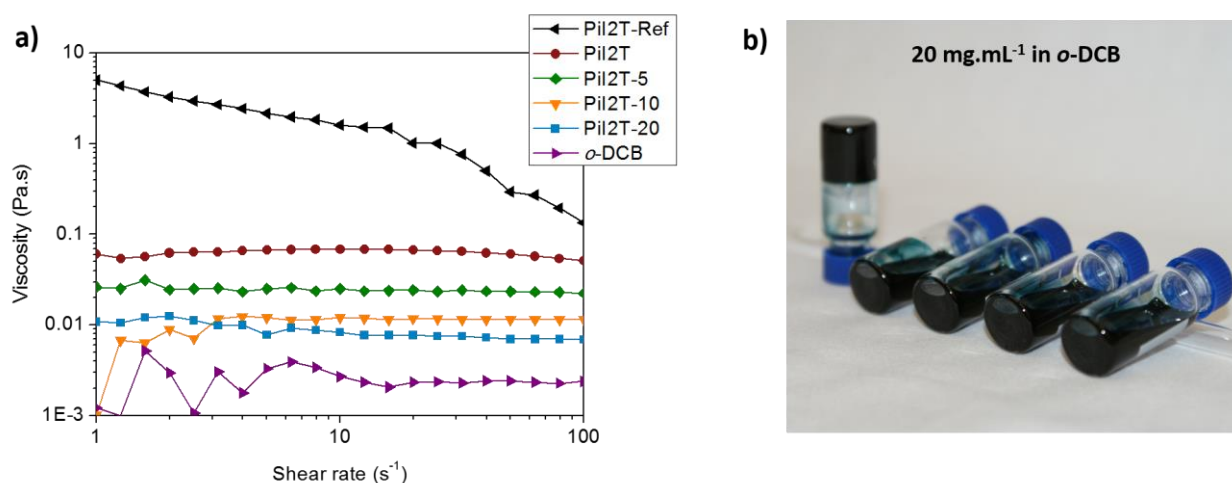


Figure 1. (a) Flow curves of the different **PiI2T-X** polymers and *o*-DCB. (b) Photograph of **PiI2T-Ref**, **PiI2T**, **PiI2T-5**, **PiI2T-10** and **PiI2T-20** (back to front) solutions in *o*-DCB (20 mg.mL⁻¹).

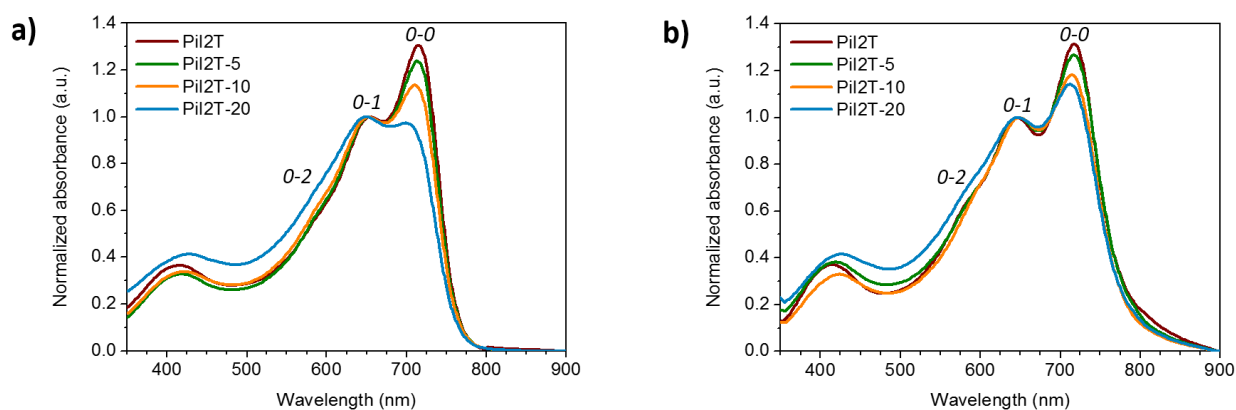


Figure 2. (a) Normalized UV-*vis.* absorption spectra of the various **PiI2T-X** polymers in dilute ($\sim 10^{-6}$ M) chlorobenzene solution and (b) thin film spin-coated on glass from 10 mg.mL^{-1} in chlorobenzene.

Table 2. Electrochemical properties of the **PiI2T-X** polymers.

Polymer	IP_{CV}^a [eV]	IP_{DPV}^b [eV]	E_g^c [eV]	EA_{CV}^d [eV]	EA_{DPV}^e [eV]
PiI2T	-5.46	-5.56	1.58	-3.88	-3.98
PiI2T-5	-5.44	-5.57	1.59	-3.85	-3.98
PiI2T-10	-5.48	-5.57	1.58	-3.90	-3.99
PiI2T-20	-5.42	-5.56	1.58	-3.84	-3.98

^a Ionisation potentials measured by cyclic voltammetry. ^b Ionisation potentials determined by differential pulse voltammetry. ^c Optical bandgap obtained from the absorption onset of the UV-*vis.* absorption spectra of polymer thin films on glass. ^d Electron affinity, obtained by summarizing IP_{CV} and E_g . ^e Electron affinity, obtained by adding E_g to IP_{DPV} .

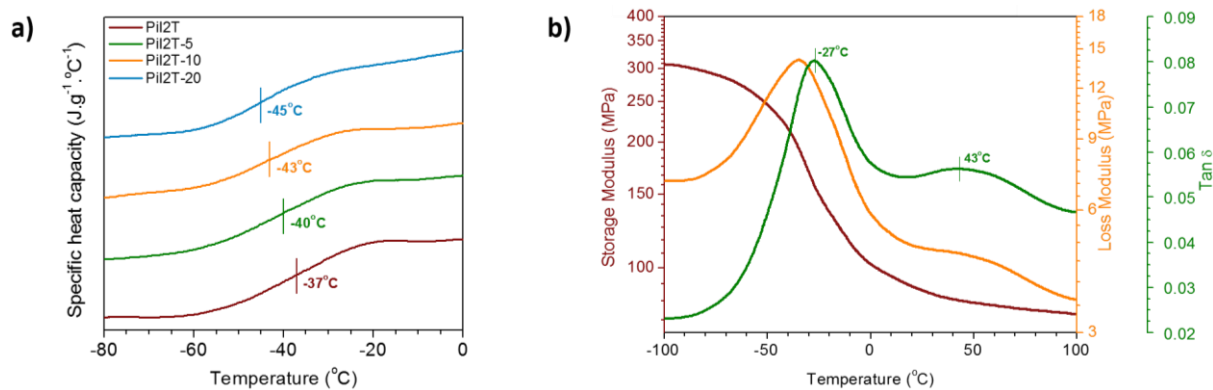


Figure 3. (a) DSC heating traces of the different **PiI2T-X** polymers (endothermic signals are positive). (b) Storage and loss moduli, as well as $\tan \delta$, of **PiI2T** measured by DMA.

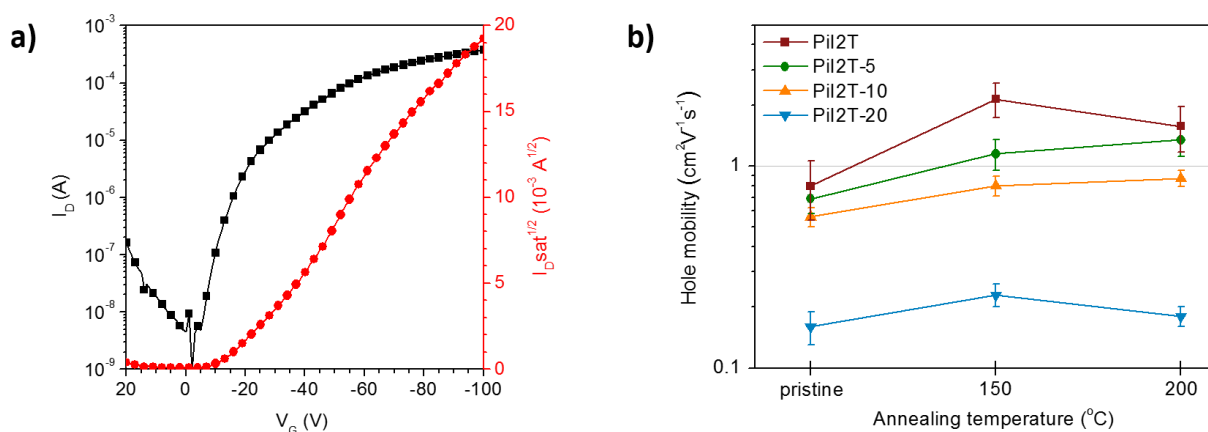


Figure 4. (a) **PiI2T-5** transfer curves after annealing at 200°C and (b) evolution of hole mobilities of all **PiI2T-X** polymers as a function of annealing temperature.

Table 3. OFET device characteristics of the **PiI2T-X** polymers. ^a

Polymer	Annealing temp. [°C] ^b	μ_h (μ_h^{\max}) [cm ² .V ⁻¹ .s ⁻¹]	$I_{\text{on}}/I_{\text{off}}$	V_{th} [eV]
PiI2T	as-cast	0.80 ± 0.26 (1.12)	~10 ⁷	-35.5 ± 1.9
	150	2.15 ± 0.41 (2.86)	~10 ⁷	-43.3 ± 4.2
	200	1.58 ± 0.40 (2.30)	~10 ⁷	-40.5 ± 4.1
PiI2T-5	as-cast	0.69 ± 0.11 (0.92)	~10 ⁶	-35.3 ± 1.1
	150	1.15 ± 0.20 (1.45)	~10 ⁷	-38.4 ± 1.3
	200	1.35 ± 0.23 (1.72)	~10 ⁶	-36.2 ± 2.8
PiI2T-10	as-cast	0.56 ± 0.06 (0.73)	~10 ⁵	-34.6 ± 1.7
	150	0.80 ± 0.09 (0.91)	~10 ⁶	-41.8 ± 3.1
	200	0.87 ± 0.08 (1.01)	~10 ⁵	-36.7 ± 1.6
PiI2T-20	as-cast	0.16 ± 0.03 (0.21)	~10 ⁷	-37.1 ± 4.9
	150	0.23 ± 0.03 (0.27)	~10 ⁵	-37.4 ± 2.8
	200	0.18 ± 0.02 (0.21)	~10 ⁷	-35.4 ± 4.1

^a All values presented are average values, extracted from at least 6 devices. ^b Annealed at the given temperature during 1 hour under protective nitrogen atmosphere.

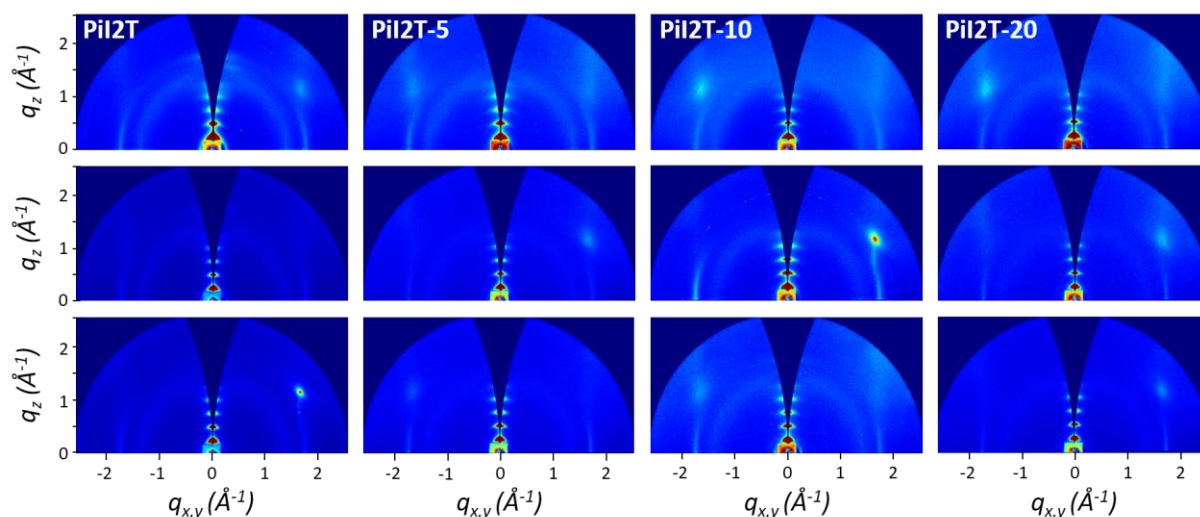


Figure 5. Two dimensional grazing incidence X-ray diffraction (GIXD) patterns of the different **PiI2T-X** polymers spin-coated from 10 mg/mL chlorobenzene solutions on Si/SiO₂ substrates. (top row) pristine thin films, (middle row) after annealing at 150°C,

respectively (bottom row) at 200°C for 1 hour under protective nitrogen atmosphere. The occasional bright spots apparent on the images ($Q_{xy} = 1.7$ and $Q_z = 1.2$) are due to diffuse scattering from the Si substrates and are often observed.

Table 4. Crystallographic parameters for all **PiI2T-X** polymers.

Polymer	Annealing temp. [°C]	Lamellar spacing [Å]	Lamellar peak FWHM [1/ Å]	π - π spacing [Å]	π - π peak FWHM [1/ Å]
PiI2T	pristine	24.36	0.0458	3.560	0.1390
	150	24.26	0.0245	3.549	0.1214
	200	24.18	0.0213	3.556	0.1296
PiI2T-5	pristine	24.19	0.0367	3.571	0.1193
	150	24.10	0.0233	3.566	0.1112
	200	24.04	0.0215	3.582	0.1125
PiI2T-10	pristine	23.92	0.0304	3.574	0.1214
	150	23.91	0.0228	3.564	0.1085
	200	23.87	0.0202	3.570	0.1072
PiI2T-20	pristine	23.67	0.0353	3.576	0.1336
	150	23.69	0.0232	3.589	0.1177
	200	23.61	0.0220	3.587	0.1013

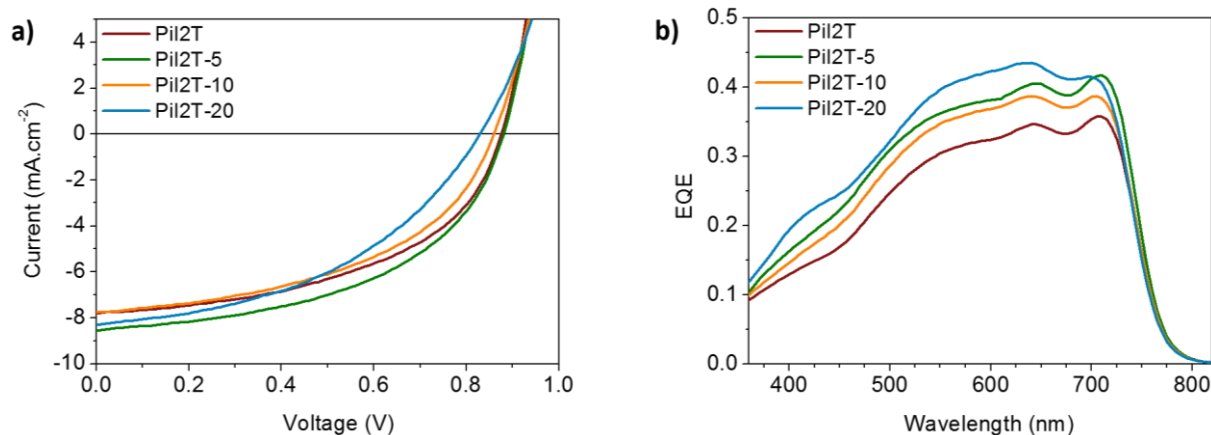


Figure 6. (a) J - V curve and (b) EQE spectra of all-polymer solar cells using **PiI2T-X** as donor and **P(TP)** as acceptor polymer.

Table 5. Photovoltaic parameters of the **PiI2T-X** polymer based all-polymer solar cells (averaged over 20 devices).

Polymer	V _{oc} [V]	J _{sc} [mA.cm ⁻²]	FF	PCE [%]
PiI2T	0.87	7.77	0.49	3.3
PiI2T-5	0.87	8.51	0.50	3.7
PiI2T-10	0.85	7.83	0.48	3.2
PiI2T-20	0.83	8.30	0.44	3.0

Understanding the viscoelastic properties of organic semiconductors is crucial in order to fabricate large-area, flexible electronic devices via solution printing. Herein the synthesis and detailed study of viscoelastic properties of a series of highly soluble isoindigo based polymers is presented. By introducing non-conjugated flexible linkers into the polymer backbone, the processability of the materials can be tuned without sacrificing the device performance.

Bob C. Schroeder, Yu-Cheng Chiu, Xiaodan Gu, Yan Zhou, Jie Xu, Jeffrey Lopez, Chien Lu, Michael F. Toney and Zhenan Bao*

Non-conjugated flexible linkers in semiconducting polymers – a pathway to improved processability without compromising device performance

